Feasibility Study on Aluminum Alloys and A441 AISI Steel Joints by Friction Stir Welding

H. Aghajani Derazkola*
Department of Engineering,
Islamic Azad University of Sari Branch, Iran
E-mail: h.aghajany@gmail.com
*Corresponding author

M. Elyasi
Department of Mechanical Engineering,
Babol Noshiravani University of Technology, Iran
E-mail: elyasi@nit.ac.ir

M. Hossienzadeh
Department of Engineering,
Islamic Azad University of Ayatollah Amoli branch, Iran
E-mail: m_hoseinzadeh@yahoo.com

Abstract: In this paper, welding feasibility between AA1100, AA5050 and AA6082 aluminum alloys and A441 AISI steel by friction stir welding has been studied. For this purpose, numerical simulation of heat generation, material flow, defect formation, tensile and micro-hardness test were investigated on all joints. The numerical simulation results indicates that the maximum heat generated in AA6082 and AA441 AISI joint and heat distribution on AA1100 surface is more than other joint planes. The optical microscope images revealed that the stir zone in AA1100-A441 AISI has linear shape, whereas the other joints have elliptical shape. The AA1100-A441 AISI stir zone made defect free, meanwhile small tunnel were formed in the stir zone of AA6082, AA5050 and A441 AISI joints. The failure position on the tensile specimens was located at the aluminum side on all joints. The tensile test shows that the uppermost joint efficacy was allocated to AA6082 - A441 AISI. The micro-hardness tests indicates that the stir zone have superior hardness with respect to the other weld areas. This phenomenon is the consequence of distributed steel fragments in stir zone and formation of intermetallic compounds in Al/St interfaces.

Keywords: A441 AISI, Aluminum Alloys, Friction Stir Welding, Material Flow, Mechanical Properties, Thermal Analysis

Biographical notes: H. Aghajani Derazkola received his MSc in Mechanical Engineering from Islamic Azad University of Sari branch in 2014. **M. Elyasi** is Assistant Professor at the Department of Mechanical Engineering, Noshiravani University of technology, Babol, Iran. His current research interest includes metal forming, composites and advance processes in metal joining. **M. Hoseinzadeh** is Assistant Professor of Mechanical engineering at the Islamic Azad University of Aiattloah amoli branch, Iran. His current research focuses on tube drawing and advanced processes in metal joining.

1   INTRODUCTION

Friction stir welding (FSW), is a solid state joining process that was invented in 1991 by TWI for welding of aluminium alloys [1]. In this process, a non-consumable rotating tool with a probe, is plunged into the seam between two workpieces to be joined. Local heating caused by friction between the tool and the workpiece reduces the flow stress of the material, and upon translation of the tool, the softened material is plastically deformed by the rotating pin [2]. The thermo-mechanical process during friction stir welding results in the change in the distribution, size and density of the precipitates in various zones [3].

The temperature reached in the nugget zone (NZ) is sufficiently high to induce the dissolution of the hardening precipitates [4-7]. The two sides of the NZ are commonly referred to as the thermo-mechanically affected zone (TMAZ), which experiences lower heat input and smaller plastic deformation. Outside of the TMAZ is the heat affected zone (HAZ), which is subjected only to the thermal cycle. Generally, the base metal (BS) is the area that doesn't experience any changes [8-9].This process is schematically shown in Fig. 1.
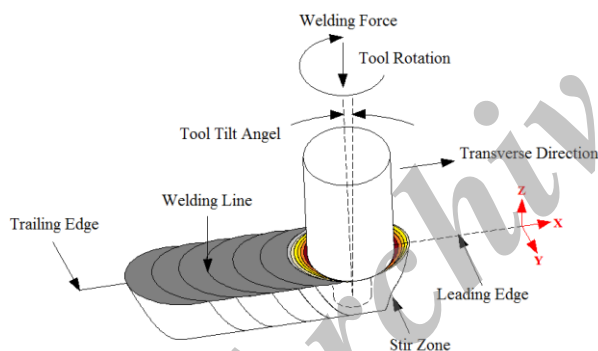

Fig. 1   Friction stir welding illustration

In the absence of filler metal in FSW joints, structures with more strength, higher corrosion resistance and lower weight can be produced. For this reasons use of FSW in offshore, aviation and rail construction has been taken into consideration in recent years. Between joints that made by FSW method, dissimilar joints between aluminum alloys and steels are widely used in low weight constructions [10-11]. Many researchers worked on friction stir welding of aluminum alloys to steels.

Elrefaey et al. [10] studied the feasibility of friction stir lap welding of a commercially aluminum plate to a low-carbon steel plate. It was reported that weld strength depended on the pin plunge depth into the steel surface. However, slight penetration of the probe tip to the steel surface significantly increased joint strength.

Kimapong et al., reported that the joint shear strength decreased with an increasing tool tilt angle and a probe diameter in friction stir welding of 5083 aluminum and SS400 steel [12]. Chen et al., investigated on the friction stir welding of AC4C cast aluminum alloy and low-carbon zinc-coated steel [13]. They reported that welding speeds had a significant effect on the tensile properties and fracture locations of the joints.

Uzun et al., studied on the joining of Al 6013-T4 alloy and X5CrNi18-10 stainless steel, which was carried out using friction stir welding technique [14]. Watanabe et al., investigated the effects of a pin rotation speed and the position for the pin axis on the tensile strength and the microstructure of the aluminum alloy and a mild steel joint [15]. The maximum tensile strength of the joint was about 86% of that of the aluminum alloy base metal. Coelho et al., jointed two different grades of high strength steel to AA6181-T4 Al alloy by friction stir welding [16]. Dehghani et al., examined Al 5186 to mild steel joint by friction stir welding technique [17]. The effects of various friction stir welding parameters were investigated on this joint. They reported that by increasing welding speed and tool rotational speed, joint tensile strength were increased. The strongest joint produced by Dehghani et al., had 90% of aluminum base alloy strength.

1XXX aluminum alloys have very low alloy elements. AA1100 has excellent characteristics in terms of thermal and electric conductivity, workability and corrosion resistance [18]. Aluminum-magnesium alloys of the 5XXX series have relatively high strength. AA5050 aluminum alloy is extensively used in structural applications, for cryogenic applications and in the naval sector [19]. AA6082 is particularly suitable to structural, architectural and decorative applications [21], where this alloy is categorized in magnesium-silicon alloys. The aim of this article is investigation of feasibility study on friction stir welding of A441 AISI steel to Aluminum alloys.

2   EXPERIMENTAL PROCEDURE

In this research AA1100, AA5050 and AA6082 aluminum alloys and A441 AISI plates with 3mm thickness were welded by regular milling machine. In the experimental process design, aluminum alloys placed advancing side, and A441 AISI as retreating side in welding fixture set on welding machine as shown in Fig. 2. Mechanical Properties of A441 AISI and aluminium alloys base metals are presented in Table 1. Welding procedure applied by hard tool which is made of Tungsten-Carbide with frustum pin, as shown in Fig. 3. The tool pin length was 3.4 mm, head diameter 4 mm, and 6 mm in beneath. The tool had 20 mm shoulder diameter.
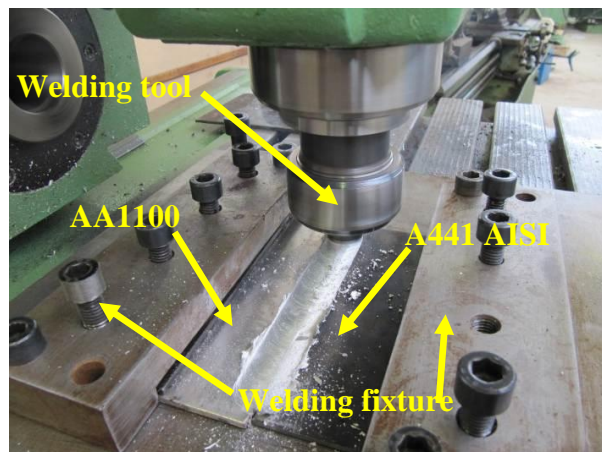
Fig. 2   FSW parts locations.

Table 1 Mechanical Properties of base metals [18]

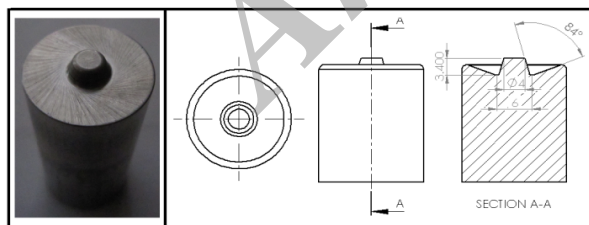|	A441 AISI	AA1100	AA5050	AA6082
ρ , kg/m^3	7800	2713	2685	2700
MP[1], ^{o}C	1400	657	652	652
K ,W/m.k	42.7	222	193	167
C$_P$, J/kg.K	477	900	898	896
σ_Y, MPa	344	34	166	267
σ_{UTS}, MPa	580	90	193	310
τ, MPa	380	62	138	207
E[2], %	15	35	24	12
VB[3]	355	23	53	95

Fig. 3   FSW frustum tool

Tool rotation direction was CCW, with 2° title angle from plate's normal surfaces and 1.5 mm offset in aluminium side. During the entire welding process, tool rotational speed was set at 710rpm and linear speeds that aluminium and steel sheets were welded together,

---

[1] Melting Point
[2] Elongation
[3] Vickers Hardness

was set at 25mm/min. To study the weld behaviour in tensile test, three samples were cut from each joint according to the ASTM E8-M03 standard by wire cut machine as shown in Fig. 4. Cross section window of welds were analysed by optical microscopy (OM) and surface material flow was observed by video measuring machine (VMM).

Fig. 4   Tensile test specimens

3   GOVERNING EQUATIONS

Heat generated by tool during the FSW process is caused by the friction and plastic deformation. In previous studies, researchers have found that only 4.5% of the total process heat is caused by plastic deformation [21]. FSW rotational tool after the initial pressure and dive into the work piece with frictional contact causes heat in the affected areas [22]. The FSW tool momentum conservation equation with forward speed on the joint line (x-axis) is defined as [21]:

$$\rho \frac{\partial u_i u_j}{\partial x_i} = -\frac{\partial P}{\partial x_j} + \frac{\partial}{\partial x_i}\left(\mu \frac{\partial u_i}{\partial x_j} + \mu \frac{\partial u_j}{\partial x_i} \right) - \rho U_1 \frac{\partial u_j}{\partial x_1} \quad (1)$$

In Eq. (1), ρ stands for density, V for linear velocity of the moving tool and P for flow pressure. In this equation, μ is a coefficient for non-Newtonian fluid, defined as ratio of the effective flow stress (σ_e) to effective strain rate ($\dot{\varepsilon}$), where this parameter is presented as follows:

$$\mu = \frac{\sigma_e}{3\dot{\varepsilon}} \quad (2)$$

As mentioned, (σ_e) is effective flow stress and ($\dot{\varepsilon}$) is strain rate, due to the material properties which can be written as follows:

$$\sigma_e = \frac{1}{\alpha} arc \sinh\left(\frac{Z}{A} \right)^{\frac{1}{n}} \quad (3)$$

In the Eq. (3), α, A and n are constants related to the base metals and Z is Zener-Holomon parameter which is defined as:

$$Z = \dot{\varepsilon} \exp\left(\frac{Q}{RT}\right) \tag{4}$$

In Eq. (4), Q is the activation energy, R is the gas constant and ($\dot{\varepsilon}$) is the effective strain rate defined as:

$$\dot{\varepsilon} = \left(\frac{2}{3}\varepsilon_{ij}\varepsilon_{ij}\right)^{\frac{1}{2}} \tag{5}$$

Where ε_{ij} is the strain rate tensor, defined as [23]:

$$\varepsilon_{ij} = \frac{1}{2}\left(\frac{\partial u_i}{\partial x_j} + \frac{\partial u_j}{\partial x_i}\right) \tag{6}$$

In welding process, the amount of torque applied on the workpieces must overcome to the maximum shear strength defined as follows [23]:

$$\tau = \frac{\sigma_y}{\sqrt{3}} \tag{7}$$

In this method, the frictional heat generation depends on the engaging surfaces between tool and workpieses. In this step, rotational pin beneath makes a hot hole that is known as technological hole. This area can also be created artificially to reduce the stresses on the FSW tool. The proportion of the maximum heat produced in FSW and workpieces melting temperature is defined by the following equation [23]:

$$\frac{T}{T_M} = K\left(\frac{\omega}{v \times 10^4}\right)^\alpha \tag{8}$$

Where α is between 0.04 to 0.06 and k is a constant selected between 0.65 to 0.75; v and ω are the tool rotational speed and welding speed respectively. According to the previous researches, the maximum temperature in friction stir welding can be about 0.6 to 0.9 base metal melting points. In this process, frictional heat generated by the tool is defined by the following equation [24-26]:

$$T = \frac{4}{3}\sqrt{\frac{\omega 2\tau 2\pi t}{\rho c K_w}} \times \frac{(D^3 + d^3)(1+P)(1+\tan\alpha)}{8}$$
$$+ \frac{K_w}{K_w + K_T \cdot \sqrt{\frac{D_w}{D_T}}} \times \frac{2\mu\pi\tau h r V}{\sqrt{3(1+\mu^2)}} + \frac{V\mu\sqrt{\pi P_M F} + 8\omega r\mu\gamma F\sqrt{V^2\omega r\sin\alpha}}{8K_w} \tag{9}$$

In this equation ρ, τ, t, K and C stand for density, shear strength, sheet thickness, thermal conductivity and specific heat respectively. While, D, d, α are tool shoulder diameter, tool pin diameter and pin angel, respectively. Also μ stands for friction, ω stands for tool rotational speed, V stands for welding travel speed, and w and T indexes stand for workpiece and tool.

During the process some of the heat generated at the interface of the tool and the work piece is wasted. This phenomenon is caused by heat transfer between the tool and the workpiece. In order to enhance the accuracy of simulation results, these parameters entered as correcting factor in Eq. (9). Finally, at the intersection of the tool and the workpiece Eq. (9) appears as below [21]:

$$q = \frac{\left(\sqrt{k\rho C_p}\right)_{workpiece}}{\left(\sqrt{k\rho C_p}\right)_{workpiece} + \left(\sqrt{k\rho C_p}\right)_{tool}} \times T \tag{10}$$

Where q_p is defined as heat generated rate per unit volume resulted as the plastic deformation outside area in the interface of workpiece and tool. This heat is about 4.5% of the total temperature engendered during FSW which is defined as follows [21]:

$$q_p = \frac{d\dot{\varepsilon}_p}{dV} = \beta\mu\varnothing \tag{11}$$

In Eq. (11), μ is coefficient of friction between the surfaces, β is the fraction of plastic deformation dissipated as heat, and ∅ is also defined as [21]:

$$\varnothing = 2\sum_{i=1}^{3}\left(\frac{\partial u_i}{\partial x_i}\right)^2 + \left(\frac{\partial u_1}{\partial x_2} + \frac{\partial u_2}{\partial x_1}\right)^2 + \left(\frac{\partial u_1}{\partial x_3} + \frac{\partial u_3}{\partial x_1}\right)^2$$
$$+ \left(\frac{\partial u_3}{\partial x_2} + \frac{\partial u_2}{\partial x_3}\right)^2 \tag{12}$$

Heat transfer between the workpiece surfaces and the tools surrounding environment as radiation and conduction is done which can be defined as:

$$-k\left.\frac{\partial T}{\partial Z}\right|_{Top} = B\epsilon\left(T^4 - T_a^4\right) + h\left(T - T_a\right) \tag{13}$$

Where T_a is ambient temperature and h is the surface heat transfer coefficient.

Table 2 Tool parameters

Tool Parameters	Value	Tool Parameters	Value
ω, rpm	710	D, mm	20
V, mm/min	25	D, mm	6
MP, °C	2500	h, mm	2.8
P, kg.m³	19400	α	84
C_P, J/kg. K	1580	μ	0.4
K, W/m.k	0.367	P, N	12e6

The heat transfer at the bottom of the tool is defined as follows:

$$k\left.\frac{\partial T}{\partial Z}\right|_{Bottom} = h_b\left(T - T_a\right) \tag{14}$$

Where h_b represents the heat transfer coefficient in beneath of tool. The above equations are written as code at MATLAB 2011 software, where the parameters used in numerical simulation are listed in Table 2.

4   RESULTS AND DISCUSSION

4.1. Heat generation and distribution

The equations described in Section 3, are used to study the effects of the position of the harder material relative to the softer material on the quality of weld temperature produced by FSW. The parameters under investigation include heat generation temperatures distribution and mechanical strain rate across the welded joint. The results are presented and discussed in this section. Fig. 5 shows the computed thermal cycles at the weld center line. It is worth mentioning that the maximum predicted temperature is about 810 °C, in welding of AA6082 to A441 AISI, while the minimum temperature is 760 °C, allocated to AA1100 to A441 AISI joint. As can be seen, the amount of frictional heat generated at the welding of AA5050 to A441 AISI is 790 °C. These results reveals that the produced temperatures are lower than the melting temperature of all sheets, which means that all the joints are developed in the solid state.
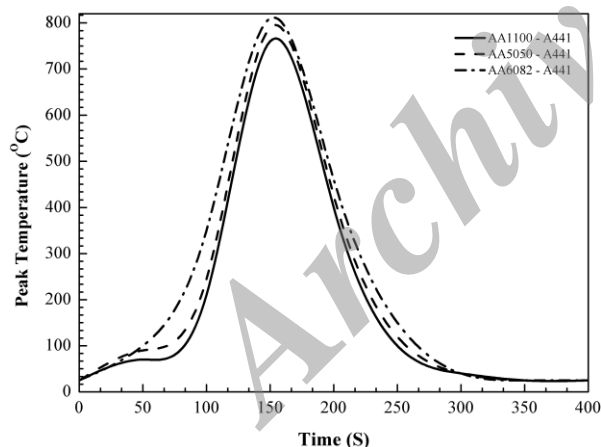

Fig. 5   Computed frictional heat generation in the joints.

The estimated temperature distribution during FSW using featured tool pin, is depicted in Fig. 6. The results show that the temperature gradient in the aluminum alloys is higher than that in the steel side irrespective of aluminum alloys positions. The temperature distribution is not similar in nature to those for similar alloy joining. This is expected because the two alloys don't have similar thermo-physical properties. The difference in alloying elements leads to differences in mechanical properties which affect the computed temperature in these cases.

Given that the mechanical parameters were considered constant for all connections, the difference of shear strength between aluminium alloys affected directly on frictional heat. In other hand, placing the A441 AISI at the advancing side resulted in slightly higher process temperatures [27-29]. Placing the harder alloy at the advancing side would create a greater tool-workpiece slippage, as a result of material flow resistance, which leads to domination of frictional heat over plastic work heat [9]. Therefore, higher temperature would be expected to develop at the surface [30]. Moreover, placing the softer material at advancing side would lead to less slippage; therefore, less frictional heat and more plastic work are produced. Due to the different heat transfer coefficient in each alloy, the temperature distribution during each welding situation will be different. During all FSW processes, temperature distribution on the steel surface was identical.
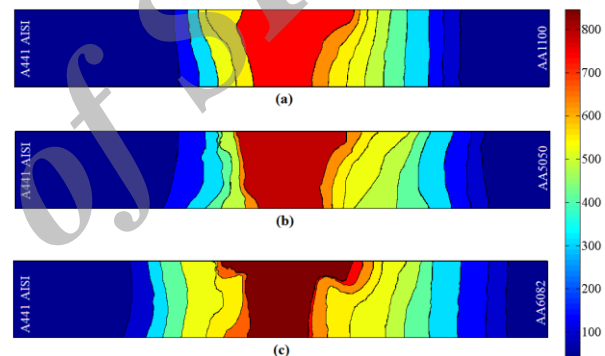

Fig. 6   Heat distribution in (a) AA1100-A441 AISI, (b) AA5050-A441 AISI and (c) AA6082-A441 AISI joints.

To better understand the heat flux in top surface of workpieces, distribution of heat in each alloy was calculated separately. Figure 7 shows the distribution of produced frictional heat in top surface of workpieces after 40s that were obtained by solving the governing equations from the MATLAB software. Surface temperature distribution in the AA1100 and A441 AAISI joint is wider than other connections. Heat distributions on the top surface of AA5050 and A441 AISI and AA6082 and A441 AISI have smaller range. This distinction in frictional heat distribution in each welding situation depends on the thermal and physical properties of the base metals. Increasing the temperature distribution results a rise in amplitude of the deformed areas while a drop in the cooling rate.

Considering the selected parameters during the simulation, 40 seconds after the linear movement of the FSW tool, 16 mm of the joint line is traversed. Due to the higher AA1100 aluminium thermal conductivity compared with other aluminium alloys, cooling rate in this base metal surface is more than other alloys. In this category, AA5050 and AA6082 are in the next rank

respectively. These characteristics emphasize that in the AA6082 and A441 AISI, microstructure changes after welding are less significant than other joints.
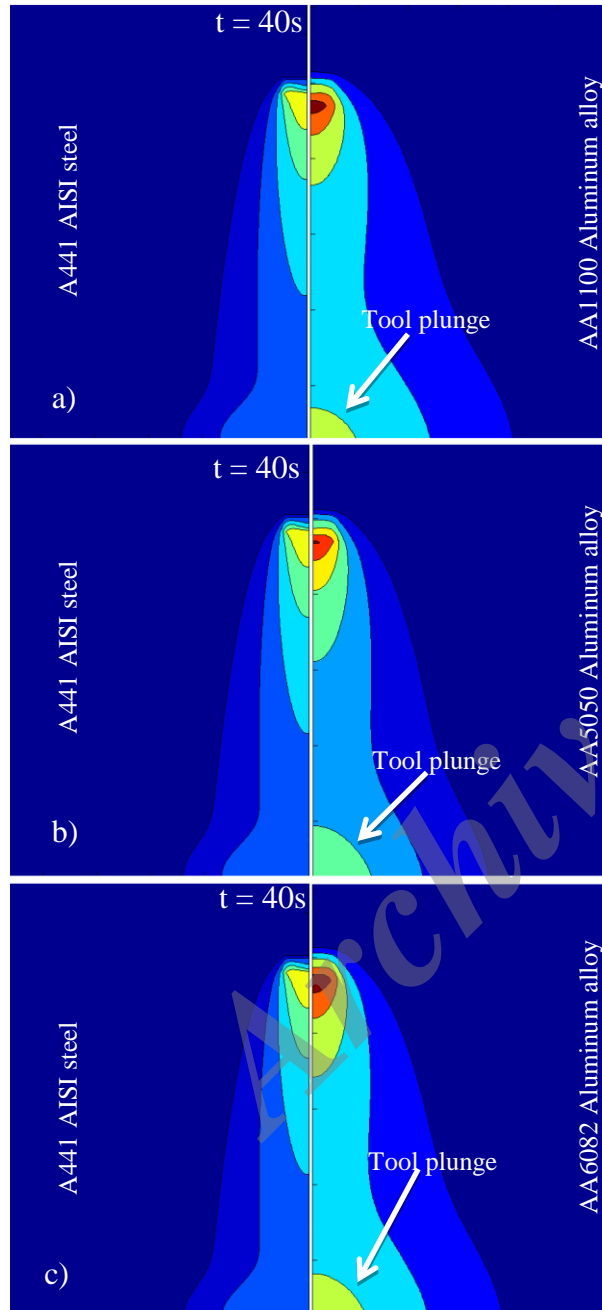

Fig. 7   Computed frictional heat generation in (a) AA1100-A441 AISI, (b) AA5050-A441 AISI and (c) AA6082-A441 AISI joints.

4.2. Analysis of the weld shapes

Figure 8 exhibit images of texture patterns on the transverse cross-section of various welds. In all these images, the A441 AISI is on the left and the aluminum alloys are on the right. In particular, Figs. 8(a), 8(b) and 8(c) expose the effect of the material stir on the texture pattern on the AA6082, AA5050 and AA1100 joints with A441 AISI steel respectively. At the first step, the shapes of the welds are analyzed, where the macro-sections reveal a zone comprising the so-called nugget zone, thermo-mechanical affected zone (TMAZ) and heat effected zone (HAZ) which is visible in aluminum sides. In the steel side only heat affected zone (HAZ) is formed. The larger part is in the upper portion of the welds revealing the key role of the shoulder on the material stirring. The thinner part is in the lower part of the weld at all joints.
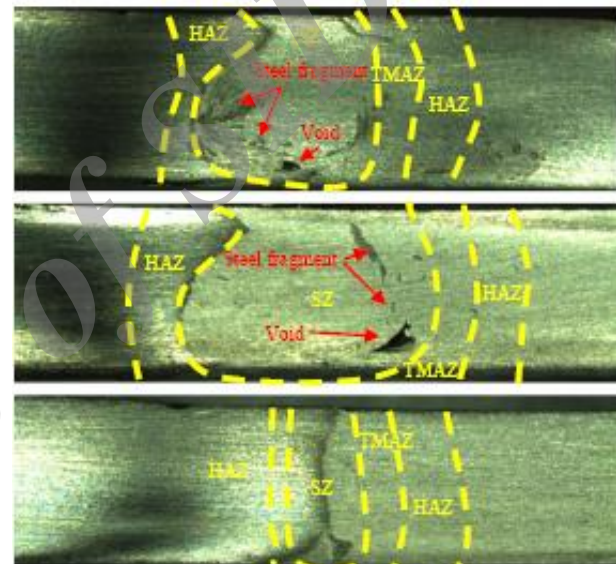

Fig. 8   Cross-sectional view of (a) AA1100-A441 AISI, (b) AA5050-A441 AISI and (c) AA6082-A441 AISI joints.

In addition, in the upper portion of each weld, the steel side and aluminum side zones are not symmetric. Differences in stir zone shape can be seen, despite the constant tool used in this study. With a quick look at each joint, it can be concluded that AA6082 - A441 AISI stir zone has circular shape, but AA5050 - A441 AISI weld has ellipsoidal stir zone. This phenomenon is related to the lower shear strength of AA5050 compared with AA6082 aluminum alloy. In both samples, the speared of fine steel fragments are visible into aluminum matrix. Between chosen aluminum alloys in this study, AA1100 alloy has lower shear strength than others. Through this weld cross section, the analyzed joint showed no evidence of mixing between the AA1100 alloy and the A441 AISI. Other recognizable characteristics in joints windows shown in Fig. 8 are layered structures and steel fragments that have been separated inside the joint transverse.

At the second step, the defects formation is analyzed. Material flow is layer wise in pin driven region and bulk flow in shoulder driven region [30]. It is understood that sound joint produced when shoulder driven material merge with pin driven material. This requires adequate temperature and hydrostatic pressure as well [30].

As can be seen in Fig. 8(a), this joint has small tunnel in the bottom of stir zone. Similarly, this defect is formed in AA5050 - A441 AISI joint as seen in Fig. 8(b). All these defects are formed in aluminum side. The main reasons of formation of these defects are related to low heat generation and improper material flow. Inappropriate material flow under this condition caused lack of surface fill, wormhole defect, or lack of consolidation [31]. Figure 8(c) shows the effect of higher heat transfer of aluminum base metal on the texture pattern for similar parameters compared with other welding samples. In this case, thermal properties of AA1100 aluminum alloy helps production of defect free joint.

4.3. Surface material flow

The horizontal view of the weld surfaces jointed in this study, are shown in Fig. 9. When the tool is traversed, the leading edge material flows to the trailing edge. During this transfer process, the plasticized material flows between tool and the relatively cooler base metal [30]. As the tool advances, material from the leading edge fills the space created due to the traverse movement, and forms the stacking of layer in the welding direction as welding progresses [30]. The material interface between the advancing side and the retreating side is clearly visible on longitudinal view. Overall, the interface is straight and parallel to the welding line.

The arc-shaped, equal-spaced banded textures are created only in the retreating side of all joints (to the right of the material interface). As shown in Fig. 9, the composition of any aluminum alloys is different with the A441 AISI steel. Surface flow of the AA6082 alloy into the A441 AISI steel is formed in the ring shape with minimal space from each other as shown in Fig. 9(a). Joint interface relative to the geometric center of stir zone, is located on the steel side. There are small holes in joint surface at aluminum side and flash bond in steel side. If the shoulder is not capable for confining the transferred material within weld nugget zone, a part of transferred material is lost as flash [30]. Hence, the shoulder driven material is not enough to fill the stir zone, leading to groove and void defects in the weld as shown in Fig. 9. AA5050 aluminum alloy and A441 AISI surface material flow is shown in Fig. 9(b).

The interface in this joint is zigzag-shaped and violently tortuous. The volume of stirred plastic material is more extensive than other welds. This issue

has led to greater connectivity of superficial ring diameter while increasing the distance between them. In the weld, joint interface has shifted slightly to the geometric central axis. Low generated heat was not able to reduce the flow stress of materials sufficiently and caused unacceptable surface flow and tunnel void in the nugget zone.
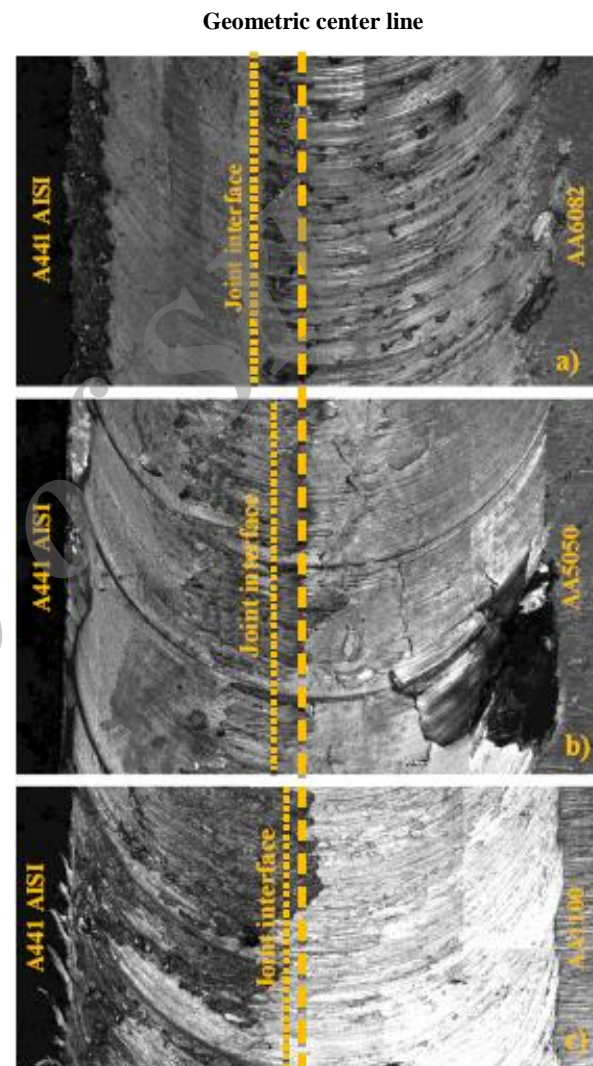

Fig. 9 Top view of (a) AA1100-A441 AISI, (b) AA5050-A441 AISI and (c) AA6082-A441 AISI joints surface flow.

Planar view of AA1100 aluminum alloy joint to A441 AISI is shown in Fig. 9(c). In particular, the interface line in this joint is discontinuous and is inserted into the space between arc-shaped bands. In this connection surface flow is in the maelstrom form. In this joint, mixing of aluminum and steel was formed layer wise and broken; while the interface between aluminum and steel was also created close to the geometric center of the sheets.

4.4. Tensile Properties

Tensile test was an important factor that indicated the weldability of aluminum alloys to A441 AISI steel. The results of tensile test indicates that ultimate tensile strength (UTS) of AA6082, AA5050 and AA1100 alloys joint to A441 AISI steel were 184 MPa, 161 MPa and 62 MPa, respectively, as shown in Fig. 10. Based on physical difference between aluminum base metals, the results do not reveal the relation between weldability of aluminum alloy to A441 AISI.
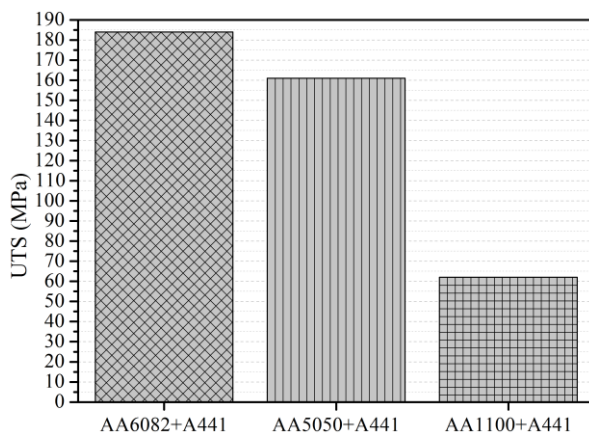

Fig. 10   Ultimate tensile strength of joints

Accordingly, in order to study the effects of tensile strength on the joints, a factor is introduced as Joint Efficacy (JE), written as follows:

$$\text{Joint Efficacy} = \frac{\text{Joint ultimate tensile strength}}{\text{Base metal ultimate tensile strength}} \times 100 \qquad (15)$$
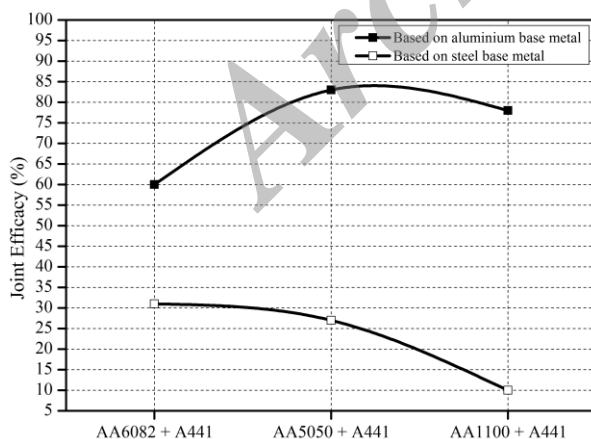

Fig. 11   Joint efficacy of A441 AISI to aluminum alloys joints

The results of JE are summarized in Fig. 11. The highest JE of FSW obtained in this study was 84% aluminum base metal, which is allocated to AA5050 to A441 AISI joint. This comparison indicated that

mingling between AA5050 to A441 AISI is more significant than other joints. Reverting to chemical composition of 5XXX alloys, manifested that the Mg element in AA5050 has good metallurgical efficacy on A441 AISI steel joint. On the other hand, it seems that Si element has inferior effect on the joint strength.

The reason for this persuasion is related to the lowest tensile strength of AA6082 joint to A441 AISI compared with AA1100 to A441 AISI which is categorized as non-alloying aluminums. As specified the JE of all joints based on steel base metal in AA6082, AA5050 and AA1100 joints are 31, 27 and 10 percent respectively. The visual observation on welds specimens shows that the fracture path location of each joint is different with others. This difference is related to the sheets materials, joint efficacy and quality of stir zone. Considering the failure location by optical microscope, specified that the AA6082 tensile specimen was broken from AL-St interface. The AA5050 and A441 AISI joint fracture location was in SZ but in AA1100 joint, the fracture path was in HAZ as shown in left side of Fig. 12.
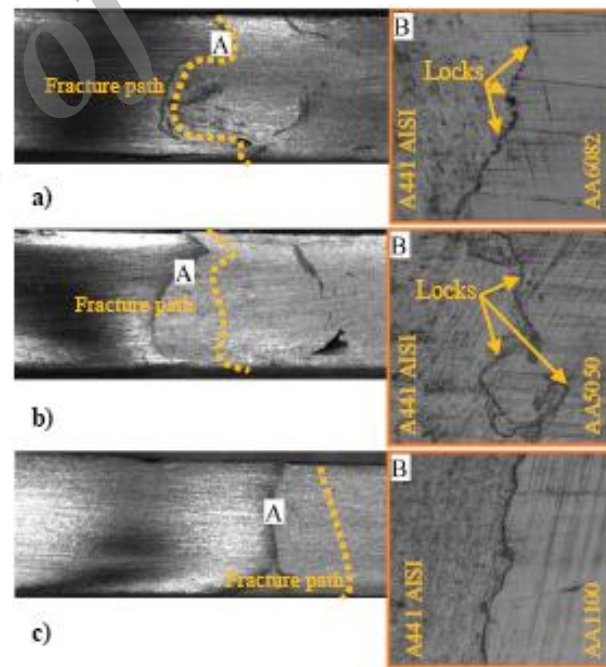

Fig. 12   A441 AISI to aluminum alloys joints fracture path.

The difference between fracture locations of tensile specimens is due to the difference in the strength of joints. Inspecting the magnified pictures indicated that some macroscopic changes have happened in sheets interface after friction stir welding. These physical changes are the result of material displacement which leads to the variation of joints strength. FSW rotating tool shifts aluminum towards steel side and

simultaneously guides the detached steel fragments to the aluminum matrix. In this situation, due to the separation of the steel fragments, the steel edges were saw-toothed. By continuing tool rotation and its forward movement, the heat source departs the stir zone and temperature drops to ambient. This process leads to a physical lock by merging the steel denote edge with aluminum base metal.

In AA6082 joint with A441 AISI the tiny dentate formed in weld interface. The physical changes in AA5050 and A441 AISI adjacent edge was more than other joints. The mechanical lock in AA5050 and A441 AISI is ripple shape. No dentate connection was observed in AA1100 to A441 AISI interface. Due to the additional softness and lower flow stress of AA1100 alloy with respect to other aluminum alloys, the metallurgical changes around FSW pin occurred quickly. These physical properties caused the generated heat to be less at welding line compared to other two joints and consequently less significant stir zone was formed in joint line. The main finding regarding the percentage of extension of the joints are summarized in Fig. 13. It can be concluded that all joints extension reveal almost the same trend as well as tensile strength. The amount of the AA6082, AA5050 and AA1100 aluminum alloys joints elongation are 1.9, 5 and 1.6 percent, respectively.
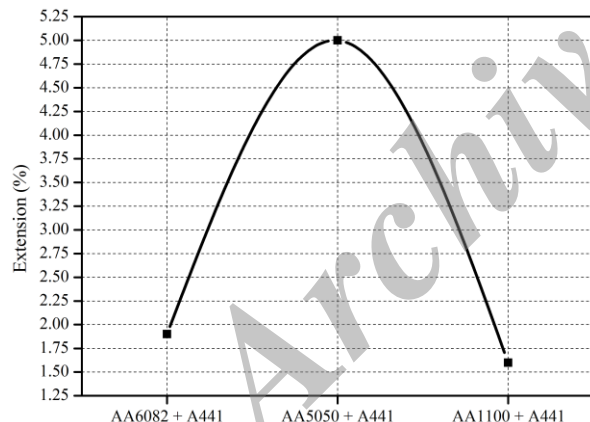

Fig. 13   A441 AISI to aluminum alloys joints extensions.

4.5. Micro-hardness

The micro-hardness profiles for different joints versus distance from the weld centre are depicted in Fig. 14. In all the cases, the hardness decreases by increasing the distance from the weld centre. The minimum amount of the hardness is located at the aluminium BMs and, by increasing the distance from this point, the hardness gradually increases, reaching the maximum hardness in SZ. In the FSW process, the thermo-mechanical cycle experienced by the material in the SZ, essentially involves hot working. The SZ is subjected to the greatest strain and strain rates as well as the highest

temperatures. These changes create appropriate condition for the formation of aluminium-steel intermetallic compounds [17].

These changes are the main reasons for increasing micro-hardness in SZ that exist in all joints. Between selected aluminium alloys in this study, interaction between AA1100 and A441 AISI was more than other joints. This phenomenon is the reason for lower tensile strength and higher SZ micro-hardness of AA1100 and A441 AISI compared to other welds. Steel fragments and structured layer formation in AA6082 and A441 AISI caused more micro-hardness compared to AA5050 and A441 AISI joint. Although the TMAZ undergoes plastic deformation, recrystallization usually does not occur in this zone owing to insufficient deformation strain [31].

However, dissolution, over-ageing, and coarsening of some precipitates are observed in the TMAZ at aluminium side, owing to high temperature exposure during the FSW process [31]. The loss of the TMAZ hardness in aluminium side compared with SZ hardness, can be attributed to the grain refinement in the SZ, caused by the intensive stirring [32]. The micro-hardness results reveals that the changes of micro-hardness at the TMAZ–HAZ interface on the steel sides are smoother than aluminium sides. This is because, the thermal cycle in the HAZ of the aluminium welds were more effective in hardness changes than steel side.
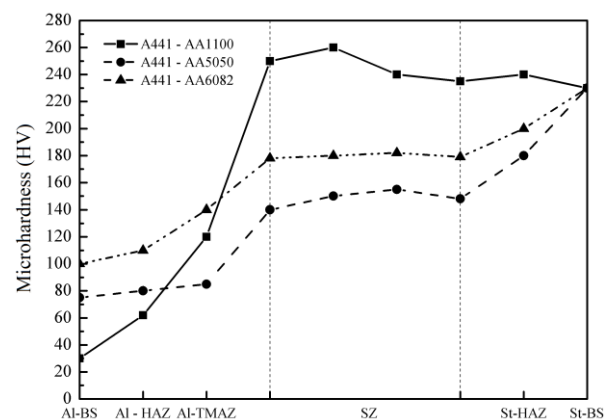

Fig. 14   A441 AISI to aluminum alloys joints
micro-hardness

5   CONCLUSION

In this research, 1XXX, 5XXX and 6XXX aluminum alloys and A441 AISI Steel were successfully welded by FSW technique. The results of the mechanical properties investigation on aluminum alloys and A441 AISI steel joint are presented below:

1- According to numerical calculations, the amount of heat generated at the junction between AA6082 and A441 AISI was higher than other welds. This is due to greater shear strength of AA6082 aluminum compared to other aluminum alloys in this study.

2- Based on numerical simulations and recorded actual temperature, heat distribution on top surface of AA1100 aluminum and A441 AISI is more significant than other connections. This is due to higher heat transfer coefficient of AA1100 aluminum than other alloys.

3- Between welded joints, FSW of AA1100 aluminum and A441 AISI has better surface material flow. Due to the low shear strength, AA1100 aluminum alloy had more vortexes. This phenomenon caused proper stir and the defect free joint in this connection.

4- AA5050 and A441 AISI joint efficacy is 85% based on aluminum base metal. The connection of AA6082 and A441 AISI joint efficacy base steel metal is larger than all joints.

5- AA1100 and A441 AISI joint interface micro-hardness is greater than other joints. This phenomenon leads to the formation of intermetallic layer in abutting edges of sheets.

REFERENCES

[1] Patil, H. S., Soman, S. N., "Influence of Weld Process Parameters on Material Characterization of Friction Stir Welded Joints of Aluminium Alloy AA6061-T6", International Journal of Advanced Design and Manufacturing Technology, Vol. 6, No. 4, 2013, pp. 9-15.

[2] London, B., Mahoney, M., Bingel, B., Calabrese, M., and Waldron, D., "Friction Stir Welding review", Proceedings of the Third International Symposium on Friction Stir Welding, Kobe, Japan, 2001, pp. 27-28.

[3] Zhang, Z., Xiao, B. L., and Ma, Z. Y., "Hardness recovery mechanism in the heat-affected zone during long-term natural aging and its influence on the mechanical properties and fracture behavior of friction stir welded 2024Al–T351 joints", Acta Materialia, Vol. 73, 2014, pp. 227-239.

[4] Sato, Y. S., Kokawa H., "Distribution of Tensile Property and Microstructure in Friction Stir Weld of 6063 Aluminum", Metallurgical and Materials Transactions A, Vol. 32A, No. 12, 2001, pp. 3023-3031.

[5] Genevois. C., Deschamps. A., Denquin. A., and Doisneau-cottignies, B., "Quantitative investigation of precipitation and mechanical behaviour for AA2024 friction stir welds", Acta Materialia, Vol. 53, No. 8, 2005, pp. 2447-2458.

[6] Liu. H. J., Fujii. H., Maedaa. M., and Nogi. K., "Tensile properties and fracture locations of friction-stir-welded joints of 2017-T351 aluminum alloy", Journal of Materials Processing Technology, Vol. 142, No. 3, 2003, pp. 692-696.

[7] Liu. F. C., Ma. Z. Y., "Influence of Tool Dimension and Welding Parameters on Microstructure and Mechanical Properties of Friction-Stir-Welded 6061-T651 Aluminum Alloy", Metallurgical and Materials Transactions A, Vol. 39, No. 10, 2008, pp. 2378-2388.

[8] Ren. S. R., Ma. Z. Y., and Chen. L. Q., "Effect of welding parameters on tensile properties and fracture behavior of friction stir welded Al–Mg–Si alloy", Scripta Materialia, Vol. 56, No. 1, 2007, pp. 69-72.

[9] Mishra, R. S., Ma, Z. Y., "Friction stir welding and processing", Materials Science and Engineering, Vol. 50, 2005, pp. 1-78.

[10] Elrefaey, A., Gouda, M., Takahashi, M., and Ikeuchi, K., "Characterization of Aluminum/Steel Lap Joint by Friction Stir Welding", Journal of Materials Engineering and Performance, Vol. 14, No. 1, 2005, pp. 48-54.

[11] Botta, S., Masetti, F., and Scanavino, S., "Overview of the applications and problems associated with the use of austeno-ferritic steels and aluminium alloys in welded structures", Welding International, Vol. 23, No. 7, 2009, pp. 530-542.

[12] Kimapong, K., Watanabe, T., "Friction stir welding of aluminum alloy to steel", Welding Journal, Vol. 83, No. 10, 2004, pp. 277-282.

[13] Chen. Y. C., Komazaki. T., Kim. Y. G., Tsumura. T., and Nakata. K., "Effect of the Surface State of Steel on the Microstructure and Mechanical Properties of Dissimilar Metal Lap Joints of Aluminum and Steel by Friction Stir Welding", Int. Welding and Joining Conf., Seoul, Korea, 2007, pp. 435-36.

[14] Uzun. H., Donne. C. D., Argagnotto. A., Ghidini. T., and Gambaro. C., "Friction stir welding of dissimilar Al 6013-T4 to X5CrNi18-10 stainless steel", Materials and Design Vol. 26, 2005, pp. 41-46.

[15] Watanabe. T., Takayama. T., and Yanagisawa. A., "Joining of aluminum alloy to steel by friction stir welding", Journal of Materials Processing Technology, Vol. 178, 2006, pp. 342-349.

[16] Coelho. R. S., Kostka. A., DosSantos. J. F., and Kaysser-Pyzalla. A., "Friction-stir dissimilar welding of aluminum alloy to high strength steels: Mechanical properties and their relation to microstructure", Materials Science and Engineering A, Vol. 556, 2012, pp. 175-183.

[17] Dehghani. M., Amadeh. A., and Akbari Mousavi, S. A. A., "Investigations on the Effects of Friction Stir Welding Parameters on Intermetallic and Defect Formation in Joining Aluminum Alloy to Mild Steel", Materials & Design, Vol. 49, 2013, pp. 433-441.

[18] Temple, P. I., "Aluminum and aluminum alloys", 10st ed., AWS Welding Handbook, Ohio, 1998, Chap1.

[19] Totten, G. E., MacKenzie, S., "Handbook of Aluminum", Vol. 2, Marcel Dekker, New York, 2003, Chap 6.

[20] Thomas, W. M. U., Nicholas, E. D., "Friction stir welding for the transportation industries", Materials & Design, Vol. 18, No. 4, 1997, pp. 269-273.

[21] Nandan, R., Roy, G. G., Lienert, T. J., and DebRoy, T., "Numerical modelling of 3D plastic flow and heat transfer during friction stir welding of stainless steel", Science and Technology of Welding and Joining Vol. 11, No. 5, 2006, pp. 526-537.

[22] Frigaad, O., Grong, O., and Midling, O. T., "A process model for friction stir welding of age hardening aluminum alloys", Metallurgical and materials transactions A, Vol. 32, 2001, pp. 1189-1200.

[23] Nandan, R., Roy, G. G., and Debroy T., "Numerical Simulation of Three-Dimensional Heat Transfer and Plastic Flow during Friction Stir Welding", Metallurgical and materials transactions A, Vol. 37A, 2006, pp. 1247-1259.

[24] Aghajani Derazkola, H., Elyasi, M. "Thermal Modeling of Friction Stir Welding Tool", 21st Annual International Conference on Mechanical Engineering-ISME2013, Tehran, Iran.

[25] Aghajani Derazkola, H., Elyasi, M., "Frictional temperature analysis in Friction Stir welding", 7st National student Conference on Mechanical Engineering-STU2013, Tehran, Iran.

[26] Aghajani Derazkola, H., Elyasi, M., and Hoseinzadeh, M., "A new thermal model in friction stir welding process", Journal of modarres mechanic (to be published).

[27] Dubourg. L., Merati. A., Jahazi. M., "Process optimisation and mechanical properties of friction stir lap welds of 7075-T6 stringers on 2024-T3 skin", Materials & Design, Vol. 31, 2010, pp. 3324-3330.

[28] Ericsson. M., Sandstrom. R., "Influence of welding speed on the fatigue of friction stir welds, and comparison with MIG and TIG", International Journal of Fatigue, Vol. 25, 2003, pp. 1379-1387.

[29] Moreira. P., De Figueiredo. M., and De Castro. P., "Fatigue behaviour of FSW and MIG weldments for two aluminium alloys", Theoretical and Applied Fracture Mechanics, Vol. 48, 2007, pp. 169-177.

[30] Arbegast. W. J., "A flow-partitioned deformation zone model for defect formation during friction stir welding", Scripta Materialia, Vol. 58, 2008, pp. 372-376.

[31] Kumar. K., kailas. S. V., "The role of friction stir welding on material flow and weld formation", Material science and engineering A, Vol. 485, 2008, pp. 367-374.

[32] Aydin. H., Bayram. A., Uguz. A., and Akay. K. S., "Tensile properties of friction stir welded joints of 2024aluminum alloys in different heat-treated-state", Materials & Design, Vol. 30, No. 6, 2009. pp. 2211-2221.

[33] Bahemmat. P., Haghpanahi. M., Besharati. M. K., Ahsanizadeh. S., and Rezaei. H., "Study on mechanical, micro-, and macrostructural characteristics of dissimilar friction stir welding of AA6061-T6 and AA7075-T6", Proc. IMechE Part B: J. Engineering Manufacture, Vol. 224, pp. 1854-1865.